Nanoscale

Accepted Manuscript

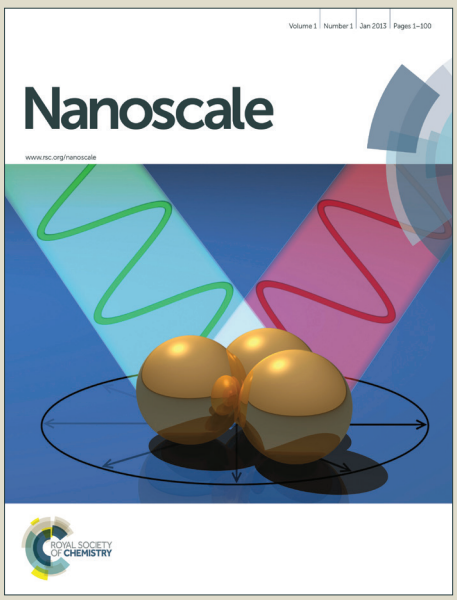

ROYAL SOCIETY OF CHEMISTRY

www.rsc.org/nanoscale

Journal Name

RSCPublishing

ARTICLE

Tin-decorated ruthenium nanoparticles: a way to tune selectivity in hydrogenation reaction

Cite this: DOI: 10.1039/x0xx00000x

Received 00th January 2012,
Accepted 00th January 2012

DOI: 10.1039/x0xx00000x

www.rsc.org/

Eric Bonnefille,[a,b] Fernando Novio,[a,b] Torsten Gutmann,[a,b] Romuald Poteau,[c] Pierre Lecante,[d] Jean-Claude Jumas,[e] Karine Philippot*[a,b] and Bruno Chaudret*[c]

Two series of ruthenium nanoparticles stabilized either by a polymer (polyvinylpyrrolidone; Ru/PVP) or a ligand (bisdiphenylphosphinobutane; Ru/dppb) were reacted with tributyltin hydride [(n-C_4H_9)$_3$SnH] to lead to tin-decorated ruthenium nanoparticles, Ru/PVP/Sn and Ru/dppb/Sn. The Sn/Ru molar ratio was varied in order to study the influence of the surface tin content on the properties of these new nanoparticles, by comparison with Ru/PVP and Ru/dppb. Besides HREM and WAXS analyses, spectroscopic techniques (IR, NMR and Mössbauer) combined with theoretical calculations and a simple catalytic test (styrene hydrogenation) allowed us to evidence the formation of μ^3-bridging "SnR" groups on the ruthenium surface as well as to rationalize their influence on surface chemistry and catalytic activity.

Introduction

Metal nanoparticles in the range 1-10 nm are of high interest in catalysis due to their high number of surface atoms and consequently, their high number of potential active sites which may exhibit electronic properties different from both those of molecular species and of bulk materials.[1] However, in order to explore in depth these advantages, it is necessary to synthesize metal nanoparticles of reproducible characteristics that will lead to constant properties. In our team, we have been working for over 20 years on the synthesis of metal nanoparticles through an organometallic approach.[2] By this technique, we are able to produce small and well-controlled metal nanoparticles, the surface of which is only covered by hydrides resulting from the reaction conditions (decomposition of organometallic precursors under dihydrogen) and organic molecules that are added as stabilizers.[3]

The choice of the stabilizing agent (polymer, ionic liquid, alcohol, amine, silane, phosphine, sulfur, carbene…) is crucial as it will influence the characteristics of the particles, not only their surface properties but also their structure (size, shape, chemical composition). Thus, since the catalytic properties of metal nanoparticles are related to their mean size, surface state and/or structure, it should be possible to tune their catalytic performance by an appropriate choice of the stabilizing ligands. In the modern area of nanocatalysis, this aspect is today investigated by the scientific community all over the world by using simple ligands or more sophisticated ones to orientate metal nanoparticle surface properties and increase reactivity and/or selectivity of the nanocatalysts in target catalytic reactions.[1e]

In contrast to the use of ligands to decorate metal nanoparticles and modulate their surface chemistry, the interaction of metal complexes with the surface of nanoparticles is not well developed. This may arise from the fact that the researchers are more interested in the direct synthesis of bimetallic nanoparticles (alloy or core-shell), as it is well-known that one can expect new properties (selectivity, yield…) when two metals are combined in comparison to the intrinsic properties of monometallic nanoparticles.[4] Most of the bimetallic systems described are prepared by the co-decomposition of the corresponding metal salts. For example, the group of Basset [5] reported the preparation of different catalysts constituted of metal nanoparticles (Rh, Ru, Pt and Ni) supported on silica and their reactivity with an organotin species. Depending on the heating treatment after reaction with tetrabutyl tin, such catalysts accommodated some organotin fragments or adatoms at their surface and finally transformed into an alloy.

Following our previous work on the interaction of organic ligands with the nanoparticles surface and the work of Basset *et al.* on the reactivity of organometallic tin compounds with metal surface, it was of interest to try to monitor the reactivity of such tin species on nanoparticles in solution and identify their mode of coordination. A further objective was to study the

catalytic reactivity of such nanoparticles in a simple model reaction, namely hydrogenation of styrene. For this purpose, we chose ruthenium, the reactivity of which has been previously studied in the group.[6] In addition, this metal does not show any Knight shift which allows NMR monitoring of its reactivity.

Here, we report the reaction of preformed ruthenium nanoparticles (RuNPs) stabilized either by a polymer (PVP: polyvinylpyrrolidone) or by a ligand (dppb: bis(diphenylphosphino)butane) with an organometallic tin complex (tri-butyltin hydride) in order to modify their surface chemistry and further, their catalytic reactivity. We also report the full characterization of the resulting species using a combination of complementary techniques (TEM, HREM, WAXS, IR and MAS-NMR) as well as reactivity studies (CO adsorption and styrene hydrogenation), in order to obtain structural and spectroscopic information for elucidating the structure of the particles. In addition, we performed theoretical calculations (periodic DFT and virtual CPK model) that corroborate our experimental results.

To the best of our knowledge, this work is the first example of the tuning of organometallic RuNPs surface chemistry by reaction with an organotin complex and it may pave the way to orientate the catalytic properties of nanocatalysts.

Results and discussion

Synthesis of the nanoparticles and characterization by TEM/HRTEM, WAXS and Mössbauer

In this work, our main objective was to investigate the surface chemistry of tin-decorated ruthenium nanoparticles by comparison with the chemistry of pure ruthenium nanoparticles. For that purpose, we first reproduced the synthesis of pure ruthenium nanoparticles following a previously described procedure,[7] by decomposing at room temperature (r.t.) and under dihydrogen (3 bar) a THF solution of the organometallic complex [Ru(COD)(COT)] [(1,5-cyclooctadiene)(1,3,5-cyclooctatriene)ruthenium] in the presence of either a polymer (polyvinylpyrrolidone, PVP), or a bidentate diphosphine ligand, (bisdiphenylphosphinobutane, dppb) as stabilizers. The resulting samples are denoted Ru/PVP and Ru/dppb. They contain small and spherical nanoparticles of 1.3±0.2 nm and 1.7±0.3 nm (Table 1), respectively. The second step of the synthesis (Scheme 1) consisted in reacting a THF solution of both preformed Ru/PVP and Ru/dppb nanoparticles with an alkyltin complex, namely tri-n-butyltin hydride [Bu_3SnH], taking profit of the coverage of the nanoparticles surface by hydrides, owing to decomposition of the ruthenium precursor under dihydrogen. The tin complex was expected to react with the surface hydrides and to give surface tin species up to tin adatoms at the metallic surface while alkyl groups were transformed into corresponding alkanes, as, for example, in surface organometallic reactions on platinum nanoparticles deposited on supports.[5] An advantage of using such an alkyltin species is the formation of alkanes as only by-products, which are easy to eliminate under vacuum and thus limiting the pollution of the metal surface. Such experiments were then performed by reacting Ru/PVP and Ru/dppb nanoparticles with different amounts of [Bu_3SnH], namely 0.05, 0.1, 0.2 and 0.5 equiv. molar per introduced ruthenium, giving rise to new ruthenium nanoparticles incorporating tin while keeping their initial stabilizer, PVP or dppb. The purification of the nanoparticles was performed by precipitation with pentane, giving rise to solid samples. These novel nanoparticles were named Ru/PVP/Sn or Ru/dppb/Sn.

Equiv. Sn	Ru/PVP/Sn	Ru/dppb/Sn
0	1.3 ± 0.2 nm	1.7 ± 0.3 nm
0.05	1.7 ± 0.3 nm	1.6 ± 0.3 nm
0.1	1.5 ± 0.3 nm	1.7 ± 0.3 nm
0.2	1.7 ± 0.5 nm	1.7 ± 0.3 nm
0.5	1.5 ± 0.3 nm	1.6 ± 0.3 nm

Table 1. Mean sizes of Ru/PVP/Sn or Ru/dppb/Sn NPs as a function of tin amount introduced for their synthesis measured from TEM analysis.

$$\text{Ru/PVP} + Bu_3SnH \xrightarrow[\text{THF, RT}]{\text{Argon}} \text{Ru/PVP/H}_x + 3\text{-x BuH}$$

$$\text{Ru/dppb} + Bu_3SnH \xrightarrow[\text{THF, RT}]{\text{Argon}} \text{Ru/dppb/H}_x + 3\text{-x BuH}$$

Scheme 1. Synthesis of tin-decorated ruthenium nanoparticles.

The size and the composition of all Sn decorated-Ru NPs samples were characterized by TEM (transmission electron microscopy), HREM (high resolution electron microscopy), WAXS (wide angle X-ray scattering) and Mössbauer (^{119}Sn).

On TEM micrographs, Ru/PVP/Sn and Ru/dppb/Sn appear as monodisperse nanoparticles which are well-dispersed on the grid as presented for Ru/PVP/Sn and Ru/dppb/Sn obtained with 0.1 equiv. of tin complex in Figure 1.

When comparing with the initial mean size of Ru/dppb and Ru/PVP nanoparticles, the reaction of the tin complex at their surface did not lead to significant changes for the Ru/dppb system while a small difference may be observed in the case of the Ru/PVP system (Table 1). Indeed, Ru/dppb/Sn nanoparticles display a mean size in the range 1.6-1.7 nm with a standard deviation of 0.3-0.4 nm similar to the 1.7 nm initial value whatever the quantity of tin, whereas a slight size increase may be present in the case of Ru/PVP/Sn nanoparticles (mean size 1.5±0.3 nm for 0.1 and 0.5 equiv. of tin and 1.7±0.5 nm for 0.05 and 0.2 equiv. of tin).

For Ru/dppb/Sn NPs prepared with 0.1 equiv. of tin, HREM analysis revealed the presence of highly crystalline nanoparticles (Figure S1). Fourier transform (FT) of the images allowed to measure distances between atomic planes. A typical value of 0.2054 nm was found which corresponds to the theoretical distance for the (101) plane of the hexagonal close-

packed (hcp) structure of bulk ruthenium. EDX measurements indicated the presence of both Ru and Sn metals in the expected ratio when comparing with the tin amount introduced (0.1 equiv.) during the synthesis and this, for a small area of the TEM grid. This result was confirmed by quantification of metals by X-ray fluorescence experiments (Figure S2).

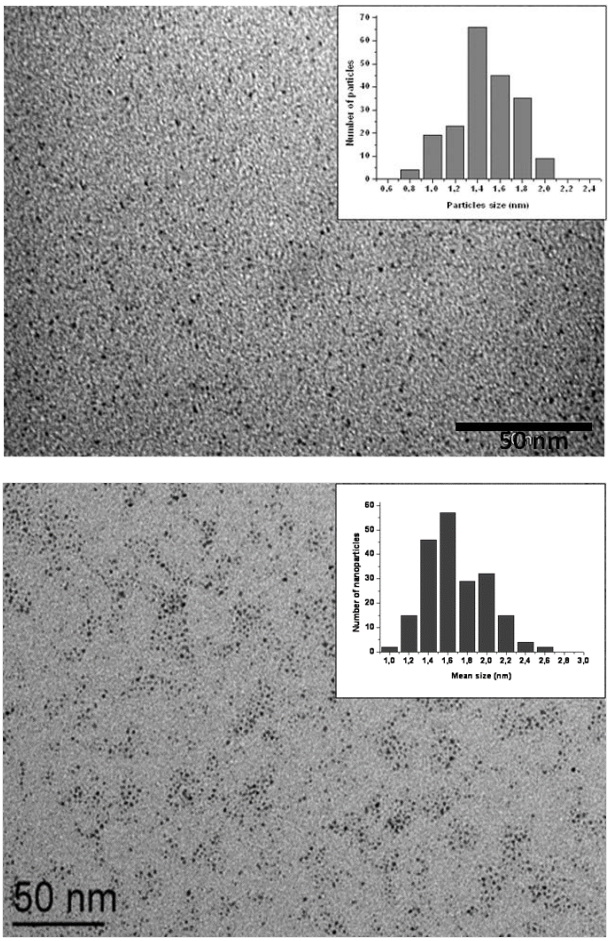

Figure 1. TEM images of Ru/PVP/Sn (Top) and Ru/dppb/Sn (Bottom) obtained with 0.1 equiv. of tin complex.

In order to fully understand the structure of these new Ru/Sn NPs, two complementary techniques (WAXS and Mössbauer) were used.

For both Ru/PVP and Ru/dppb nanoparticles, the radial distribution functions (RDFs) derived from WAXS (Wide-angle X-rays scattering) measurements on Ru/PVP/Sn and Ru/dppb/Sn are consistent with bulk ruthenium structure (Figure 2). Agreement with the RDF simulated from a spherical model based on hcp ruthenium is especially good for Ru/dppb/Sn, whilst significant distortion can be observed for Ru/PVP/Sn. The coherence lengths, which are by principle average measurements of crystalline domains, can be evaluated to 1.7 nm for Ru/dppb/Sn and 1.6 nm for Ru/PVP/Sn, in good agreement with the mean sizes derived from measurements by TEM analysis, which is also a clear indication that the nanoparticles are fully crystalline. Such a good agreement with a pure ruthenium model indicates furthermore that, especially for Ru/dppb/Sn, there is no significant diffusion of Sn inside the particles and no sign of the presence of ruthenium-tin alloy such as Ru_3Sn_7 known to display a cubic structure.[8]

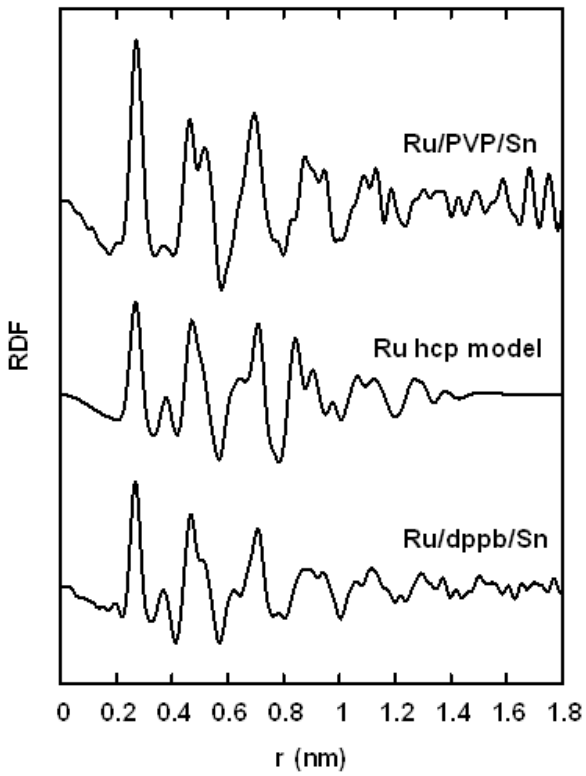

Figure 2. WAXS analysis of Ru-Sn nanoparticles- from top to bottom RDF for Ru/PVP/Sn, simulation from hcp Ru model, RDF for Ru/dppb/Sn.

^{119}Sn solid state NMR was also performed to determine the nature of tin atoms. For the Ru/PVP/Sn system prepared with the ratio of 0.5 equiv of tin, we observed a broad signal near 90 ppm (Figure 3) which is strongly shifted to low-field compared to the starting material, tri-n-butyltin hydride (- 93 ppm). This chemical shift is in agreement with the presence of tin atoms bonded to other metal atom. Although the signal to noise ratio was bad even after a long measurement time, this signal contains at least two different components with different chemical shifts. The deconvolution of the signal shown on Fig. 3 led to two bands at ca. 93 ppm and 75 ppm which can be attributed to two coordination modes of tin atoms on Ru/PVP NP surface.

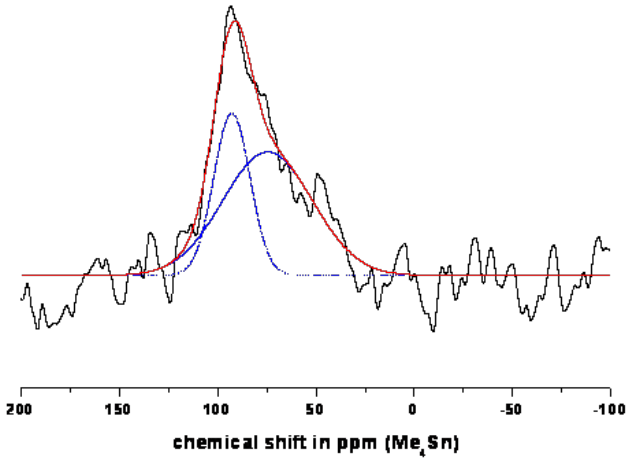

Figure 3. ^{119}Sn NMR spectrum recorded for Ru/PVP/Sn sample prepared with 0.5 equiv. of tin.

To determine the chemical environment of tin in the tin-modified RuNPs, ^{119}Sn Mössbauer spectroscopy studies were performed. This technique gives access to the oxidation state of tin and also to the nature of the atoms linked to tin. As a reference, the tri-n-butyl tin hydride precursor was first measured. It shows an isomeric shift of 1.36 mm/s with a quadrupole splitting of 0.00 mm/s and appears as an organometallic tin (IV) compound like $Sn(IV)R_4$. For Ru/dppb/Sn, ^{119}Sn Mössbauer spectra showed the presence of tetra-substituted SnR_3R' species, with an isomeric shift (IS) of 0.76 mm/s and a quadrupole splitting (Δ) of 1.90 mm/s (Figure 4). The observation of formally $Sn(IV)R_3R'$ species and the high value of quadrupole splitting indicate that the chemical environment of tin is distorted. In addition, only a tetra-substituted Sn species is present with no alloy (Ru_3Sn_7) or Sn(0) NPs.[9]

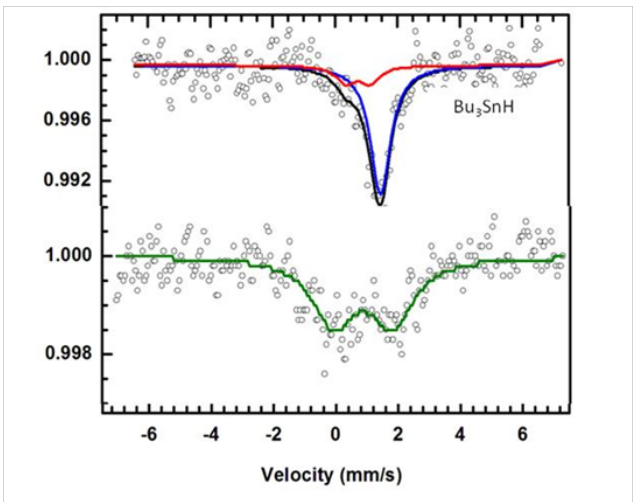

Figure 4. ^{119}Sn Mössbauer of Ru/dppb/Sn with 0.1 equiv. of tin (bottom) and Bu_3SnH (top).

To shed some light on the number of alkyl groups linked to the tin atoms, a new experiment was performed by reacting Ru/PVP nanoparticles with tri-octyltin hydride (0.1 equiv.) instead of tri-butyltin hydride, while keeping constant the other experimental conditions. By using tri-octyltin hydride it was expected to form octane molecules that can be detected by gas chromatography analysis (GC). Thus, at the end of the synthesis, decane was added as internal standard for quantitative GC analysis. This experiment was repeated three times giving rise to reproducible numbers of octane molecules released by tin atom, namely ca. 2.5. From this value it appears that two or three octyl groups could have react with the ruthenium surface, thus leading to Sn atoms linked to one or two remaining alkyl groups.

Surface investigations: quantification of surface hydrides, adsorption of CO and hydrogenation of styrene

To study the influence of the addition of tin on the surface properties of Ru/PVP and Ru/dppb nanoparticles, several reactivity experiments were carried out.

Equiv. Sn	H/Ru$_s$	
	Ru/PVP/Sn	Ru/dppb/Sn
0	1.2	0.8
0.05	1	0.6
0.1	1.1	0.8
0.2	0.1	0.8
0.5	0.05	0.7

Table 2. Quantification of surface hydrides on Ru/PVP/Sn or Ru/dppb/Sn NPs as a function of tin amount used for the synthesis.

First of all, we quantified the number of hydrides present on Ru/PVP/Sn and Ru/dppb/Sn NPs surface by a home-made titration method. This method is based on an olefin hydrogenation reaction. In a typical experiment, 2-norbornene was added to a fresh THF solution of Ru/Sn nanoparticles previously degassed by vacuum/argon cycles to eliminate any trace of dissolved dihydrogen. The conversion of 2-norbornene into norbornane was followed by GC while no dihydrogen was added, thus taking profit only of the surface hydrides to hydrogenate the olefinic double bond. Assuming a size of 1.3 nm for Ru/PVP nanoparticles, which corresponds to ca. 76 % of atoms on their surface, a value of 1.2 hydrides per surface atom was estimated [6a,7b], which is coherent with previous results for purely sterically stabilized nanoparticles (Table 2). For the Ru/PVP/Sn series, we observed that the number of surface hydrides decreased with increasing tin amount (Table 2). For a tin amount lower than 0.1 equiv., the number of hydrides is almost the same as that found for the starting Ru NPs, i.e. ca. 1.1 by surface ruthenium atom. For 0.2 equiv. of tin, we

observed a drop in the hydride content with a value of ca. 0.1H/Ru_s. For the Ru/dppb/Sn series, the calculated number of hydrides appeared lower than for the Ru/PVP/Sn samples and kept almost the same value whatever the tin amount, in the range 0.6-0.8 H/Ru_s.

In a second series of experiments, we used carbon monoxide to investigate the surface state of tin-modified RuNPs. Indeed, carbon monoxide is a molecule commonly used as a probe to study the surface chemistry on metallic surfaces, mainly by infrared spectroscopy (IR).[10] In the team, we have recently developed the investigation of the surface of Ru nanoparticles, in particular the location and dynamics of CO groups, using a combination of infrared and nuclear magnetic resonance (NMR) spectroscopic methods associated to reactivity studies.[6a,7b,11,12,13] This approach was also successful for alloyed [13c] or core-shell [13d] PtRu nanoparticles. For this purpose, in a Fischer Porter reactor, solid samples of Ru/PVP/Sn or Ru/dppb/Sn were exposed to a CO atmosphere (1 bar of ^{13}CO; 18h; r.t.). The reaction was monitored by both IR and solid state NMR spectroscopy. From recent works in the group [6a,13], we know that in these reaction conditions, CO is adsorbed on Ru/PVP NPs only in the linear coordination mode and displays a typical IR band at 1970 cm^{-1}. This was confirmed by ^{13}C solid state NMR, displaying a sharp CO resonance at 199 ppm without spinning side bands indicating the presence of very mobile CO groups on the surface of Ru/PVP NPs (Figure 5a). The signal at 175 ppm corresponds to the carbonyl function of the polymer (PVP). In the case of Ru/PVP/Sn, whatever the tin content (0.05 to 0.5 equiv. of tin), the IR studies did not show any clear carbonyl bands in the expected region for CO coordinated on RuNPs but only very weak broad band (Figures S3 and S4).

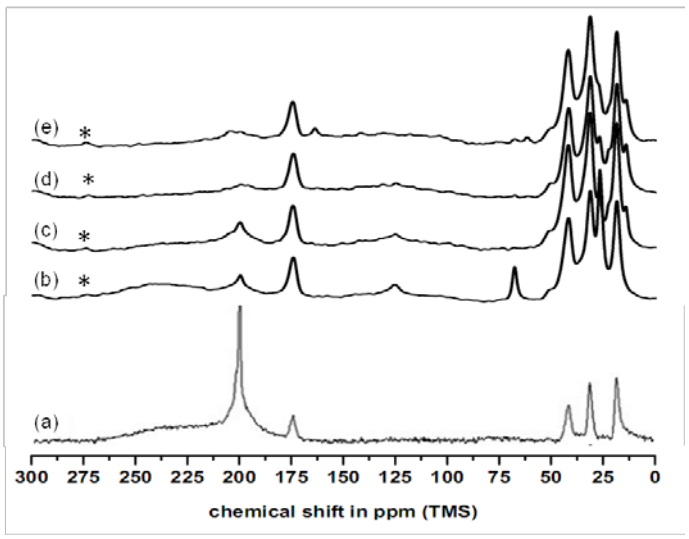

Figure 5. ^{13}C MAS NMR spectra of Ru/PVP (a) and Ru/PVP/Sn with 0.01 (b), 0.05 (c), 0.1 (d) and 0.5 (e) equiv. of tin after addition of ^{13}CO.

The ^{13}C solid state NMR spectra recorded for the Ru/PVP/Sn samples show in the C-H region of PVP three news signals at 13, 22 and 27 ppm which can be attributed to butyl groups linked to tin atoms (Figure S5). After addition of ^{13}CO, a weak broad signal is visible at ca. 200 ppm displaying spinning side bands, whatever the amount of tin deposited at the surface of the particles (0.01 to 0.5 equiv.). This signal can be attributed to linear ^{13}CO groups coordinated on the surface of the particles but which, in contrast to the Ru/PVP system, are not mobile on the surface. For the Ru/PVP/Sn/^{13}CO samples containing the lower contents of tin (0.05 equiv.), the broad signal at 200 ppm appears with an intensity higher than in the cases of 0.1 and 0.5 equiv. (Figure 5c). Furthermore, for 0.01 equiv. of tin (Figure 5b), an additional very broad signal is observed near 235 ppm which can be attributed to bridging CO groups in different chemical environments. For all Ru/PVP/Sn/^{13}CO samples, ^{1}H-^{13}C CP-MAS NMR experiments show a strong decrease of the intensity of the CO signals (Figure S6). These results evidence the absence of protons in the vicinity of the CO molecules.

Similar IR and NMR studies were carried out on the Ru/dppb/Sn system. Upon CO adsorption (Figure S7), a strong band was observed at 2001 cm^{-1}, in agreement with a linear CO coordination mode.

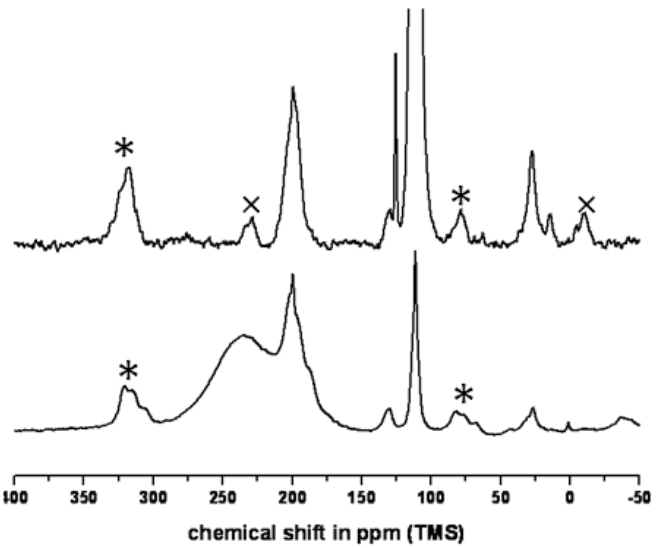

Figure 6. ^{13}C MAS NMR Ru/dppb (bottom) and Ru/dppb/Sn (top).

On the ^{13}C NMR spectra a resonance at 14 ppm corresponding to the CH_3 of butyl groups linked to tin atoms (Figure S8). Two signals are visible in the carbonyl region on the NMR spectra for Ru/dppb nanoparticles after CO adsorption (Figure 6 bottom): a sharp signal at 200 ppm and a broad signal at 230 ppm, attributed respectively to terminal and bridging CO groups. The presence of spinning side bands indicates that CO molecules are blocked in a chemical environment. Ru/dppb/Sn NPs also adsorb CO (Figure 6 top) but only a sharp signal was

observed at 199 ppm which displays spinning side bands. This signal is attributed to a linear coordination mode of CO groups, which are not mobile on the surface of these particles. The CP-MAS spectrum recorded for Ru/dppb nanoparticles evidenced a strong decrease of the CO signal due to a decrease of the number of protons close to CO molecules.[6a] For the Ru/dppb/Sn sample, MAS and CP-MAS presented the same intensity for the CO signals indicating that the number of nearby protons does not change after reaction with CO (Figure S9). ^{31}P solid state NMR (Figure S10) was also recorded for Ru/dppb/Sn prepared with 0.1 equiv. of tin. Only one broad signal was visible at ca. 50 ppm displaying spinning side bands, similarly to that previously observed for the Ru/dppb system. The presence of this low-field shifted signal compared to the free ligand indicates that the phosphorous atoms are still bound to ruthenium atoms. After reaction with ^{13}CO, the NMR spectra of Ru/dppb/Sn, did not reveal any modification of the chemical shift of phosphorus atoms.

Considering that the presence of tin atoms on the surface of Ru NPs could have an influence on their surface reactivity, the Ru/Sn systems were finally investigated as catalysts for the hydrogenation of styrene. Indeed, it is known [12] that the hydrogenation of aromatic rings requires the presence of faces while the vinyl groups can be reduced anywhere on the particles. Therefore, depending on the location of tin atoms on the surface of the RuNPs (faces, apexes or edges), differences in selectivity can be expected. In a typical experiment, 1ml of styrene was added to 0.03 mmol total of metal Ru NPs in THF inside a Fischer-Porter bottle under an argon atmosphere. Then, the reaction mixture was pressurized to 3 bar H_2 and stirred at room temperature. The results obtained after 240 h of reaction are reported in Table 3.

Equiv. Sn	**Products ratio A:B:C (%)**	
	Ru/PVP/Sn	Ru/dppb/Sn
0	0:0:100	0:0:100
0.05	0:1:99	0:95:5
0.1	0:5:95	0:88:12
0.2	0:95:5	0:99:1
0.5	15:85:0	52:47:1

Table 3. Hydrogenation of styrene with Ru/PVP/Snor Ru/dppb/Sn NPs as catalysts. Conversion determined by GC. (A=Styrene; B=Ethylbenzene; C=Ethylcyclohexane).

The Ru/PVP/Sn systems, prepared with 0.05 and 0.1 equiv of tin, led to conversions similar to those observed for pure Ru/PVP nanoparticles, namely full hydrogenation of styrene into ethylcyclohexane. These results indicate that faces are accessible to the aromatic rings. For the Ru/PVP/Sn system prepared with 0.2 equiv. of tin, only ethylbenzene was produced, thus evidencing a poisoning of the sites responsible for the hydrogenation of the aromatic ring. For a higher tin amount (0.5 equiv.), the conversion of styrene was not complete (85%). This can be explained by a higher quantity of tin atoms at the surface of the nanoparticles, probably also on edges and apexes, which would block the reaction.
In the case of Ru/dppb/Sn samples, a high selectivity in ethylbenzene was observed even for a very low amount of tin, namely 0.05 equiv. For a high tin amount (0.5 equiv. of tin), the conversion of styrene to ethylbenzene decreased to only 48%. These results may arise from the steric hindrance of the bidentate phosphine ligand on RuNPs which block apexes and thus limit the accessibility of ruthenium for hydrogenation reactions.

DFT Calculations and Virtual CPK Model

Theoretical calculations were carried out to compare with experimental data in the objective to shed some light on the structure of these tin-decorated ruthenium nanoparticles.
Periodic DFT calculations were performed to get information on the nature of tin ligands that can be coordinated on a surface of RuNPs, this having some consequences on the reactivity, number of hydrides and CO adsorption. In order to both identify the thermodynamically more stable adsorbed SnR_m species and to have an estimation of bond strengths, the following reactions were considered:

(1) $HSnR_3 + 2H^* \rightarrow SnR_3^*, 3H^*$
(2) $SnR_3^*, 3H^* \rightarrow SnR_2^*, 2H^* + RH$
(3) $SnR_2^*, 2H^* \rightarrow SnR^*, H^* + RH$
(4) $SnR^*, H^* \rightarrow Sn^* + RH$
(5) $SnR^*, H^* \rightarrow SnH^*, R^*$
(6) $Sn^*, H^* \rightarrow SnH^*$
(7) $Sn^* + ½\ H_2 \rightarrow SnH^*$
(8) $Sn^*, Me^* \rightarrow SnMe^*$

Where the * sign designates an adsorbed compound. R = -CH_3 instead of -butyl was considered as a good cost/model compromise. Reaction (1) describes the adsorption of the tin complex on a previously hydrogenated surface, accompanied by the co-adsorption of the H atom resulting from the H-Sn bond breaking. On Ru(0001) surfaces, H atoms adsorb on μ_3 sites, although we showed in previous studies that on-top and edge-bridging H atoms are present on the surface of Ru NPs.[12] Reactions (2-4) correspond to consecutive elimination reactions of -R groups from the surface, by combination with adsorbed H atoms. Additional reactions were also considered, accounting for the possible exchange between H and R in SnR* (5) and assessing the thermodynamical stability of adsorbed tin atoms (6-8).
Most of the optimized geometries are reported in Figure S11. Note that an attempt to insert a tin atom into a subsurface site of a bare surface resulted in dramatic energy convergence issues. It suggests that the presence of tin atoms under the surface is very unlikely.
The thermodynamics of these reactions are reported in Table 4. The adsorption of $HSnR_3$ (1) is exothermic by *ca*. 33 kcal/mol,

the Sn-H bond breaking being overcompensated by Ru-Sn bond formation. In the lowest isomer, **1**, the tin atom bridges a Ru-Ru bond, whereas it is on-top coordinated in **1'**, slightly higher in energy by 1.5 kcal/mol, *i.e.* almost not significant at such level of calculation. Reactions (2-4) clearly indicate that consecutive eliminations of methyl groups are thermodynamically favorable up to SnR*, whereas a final formation of Sn* is almost athermic. This energy difference of 0.6 kcal/mol suggests the possible presence of naked tin atoms on the surface, provided that the last Sn-R activation barrier is low enough. However, reaction (8) indicates a thermodynamically favorable recombination between Sn* and R groups that may be present on the surface. On the contrary, the addition of Sn* with adsorbed hydrogen atoms (6) as well as the dissociative adsorption of H_2 on Sn* (7) are both endothermic by 19.2 kcal/mol and 5.2 kcal/mol. Reactions (3) and (4) were also investigated on an hcp 55-atom model cluster. The energy yields are similar to those obtained on the regular surface.

Reaction	ΔE/ kcal.mol^{-1}
(1)	-33.1
(2)	-12.7
(3)	-10.8
(4)	0.6
(5)	23.5
(6)	19.2
(7)	5.2
(8)	-4.1

Table 4. Energies for reactions (1-5). The lowest adsorbed configuration, 1, was considered for reactions (1) and (2).

Ligands spread over the surface of NPs according to electronic as well as to steric effects. Since surfaces of middle transition metals are strongly electron-deficient, the number of surface ligands is to some extent ruled by steric hindrance. The number of -$SnBu_3$ ligands that could occupy the surface of ~ 1.9 nm hcp Ru NP has been estimated using an home-made program based on a hard sphere model [13a]. Three likely structures are shown on Figure 7. **6** and **7** are representative of RuNPs dressed respectively by stretched out conformers of -SnBu3 and their less bulky counterparts, *i.e.* with vertically oriented butyl groups. These simulations indicate that such ~ 300 ruthenium atoms-NPs could accommodate approximately 0.035 and 0.055 equivalent of tin on their surface. It is obvious that more -SnBu ligands can be adsorbed on the surface without experiencing any steric discomfort. With such ligand, the metal surface in **8** is dressed by *ca.* 0.1 equivalent of tin.

DFT calculations indicate that Ru_3-SnBu is the most stable structure (Figure 8) and virtual CPK models demonstrate that 28 μ_3-*SnBu* can be located on a Ru NP of 1.9 nm, *i.e.* one Sn per Ru or 0.15 Sn per surface Ru atom.

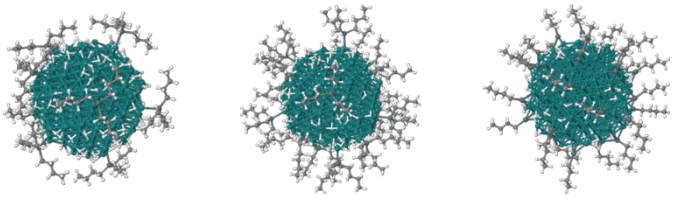

Figure 7. Grafting on a 1.9 nm hcp Ru NP (Ru_{288}) of 10 top-h-$SnBu_3$, **6**, 16 top-v-$SnBu_3$, **7**, or 28 μ_3-SnBu, **8**. Some hydrides were also added to remind their presence on the surface.

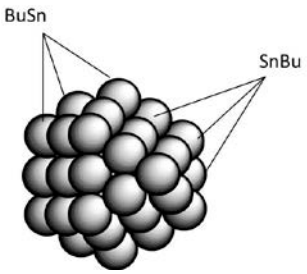

Figure 8. Schematic representation of the coordination of tin on RuNPs resulting from DFT calculations.

Discussion

The reaction of preformed Ru/PVP and Ru/dppb nanoparticles containing surface hydrides with different amounts of tri-n-butyltin hydride [Bu_3SnH] complex gave rise to new ruthenium nanoparticles that are decorated with tin atoms at their surface. By using a combination of different analytical techniques as well as theoretical modeling we could show that these particles adopt the hcp structure of bulk ruthenium and no evidence was found for the formation of any RuSn alloy or for the presence of Sn nano-crystallites. In addition, since neither the mean size nor the lattice parameters of the RuNPs are altered, the deposition of tin is proposed to occur only at the surface of the particles.

The ^{31}P solid state NMR spectrum of Ru/dppb/Sn is similar to that of Ru/dppb NPs, indicating that the phosphorous atoms are still coordinated to ruthenium atoms. The ^{119}Sn broad and low-field shifted signal observed for Ru/PVP/Sn NPs is in agreement with tin bonded to a metal atom and the fact that it contains two different components is in accordance with two coordination modes of tin atoms with Ru/PVP NPs surface. Although the origin of the presence of these two peaks displaying a slightly different chemical shift but a very different line shape was not elucidated, they both could correspond to two tin tetracoordinated species, for example a terminal SnR3 and a triply bridging SnR moieties. However, ^{119}Sn Mössbauer for both Ru/PVP/Sn and Ru/dppb/Sn revealed the presence of only one tetra-substituted tin species of the type SnR_3R'. From the complementary reaction of Ru/PVP NPs with tri-octyltin hydride, the reactivity of which is similar to that of tri-butyltin hydride, we know that ca. 2.5 octane molecules are released per tin atom. This could translate into the formation of essentially

triply bridging Sn-R groups associated to some less decomposed species such as some terminal SnR_3 groups. This hypothesis is supported with DFT calculations which show the tendency for the trialkyltin hydride complexes to form surface triply bridging species.

The titration of the surface hydrides revealed a very interesting discrepancy between Ru/PVP and Ru/dppb. A decrease of hydride number with increasing tin amount was observed for the Ru/PVP/Sn series (from 0.05 H/Ru_s to 1.1 H/Ru_s) while for the Ru/dppb/Sn series, the quantity of hydrides is lower than for Ru/PVP/Sn system but almost constant whatever the tin amount. This can be related to the fact that Ru/PVP/Sn cannot accommodate CO after the addition of even a very small amount of tin while Ru/dppb/Sn can still accommodate terminal CO groups. These observations can both arise from the sterical hindrance of the dppb ligand. Indeed, this ligand is very bulky and may cover a large part of the surface of the Ru/dppb NPs. This could limit the reaction of the also bulky tin hydride molecules with the nanoparticle surface. In this case, only the faces, not protected by dppb would rapidly lose their hydrides and their capability to coordinate CO in a bridging mode. The hydrides, and after carbonylation, the terminal CO located near the phosphines would still be present. In summary, in the absence of coordinating ligands on their surface Ru/PVP nanoparticles are rapidly covered with tin whereas tin coverage is limited to the open face areas in the case of Ru/dppb. It is then interesting to find out how this behavior translates in terms of catalytic reactivity.

Thus, the results obtained in hydrogenation of styrene also evidenced important differences between Ru/PVP/Sn and Ru/dppb/Sn nano-catalysts. The Ru/PVP/Sn NPs showed a gradual variation of selectivity with increasing tin loading while only a small quantity of tin was sufficient to impede the arene hydrogenation ability of Ru/dppb nanoparticles. It is noteworthy that these observations fit the modeling studies, since the virtual CPK model has suggested that 28 μ_3-*SnBu* can be located on a RuNP of ~1.9 nm (262 Ru atoms: 167 on the surface and 95 in the core). Considering the 1.5 nm mean size of the Ru/PVP/Sn NPs (130 Ru atoms: 98 on the surface and 32 in the core) by correlation with the CPK model, we can calculate that ca. 16 tin atoms can be coordinated on their surface. When using 0.1 equiv. of tin we can estimate that ca. 13 tin atoms are introduced during the synthesis of Ru/PVP/Sn NPs. So, for 0.1 equiv. of tin, the surface of Ru/PVP NPs should not be saturated and therefore can still hydrogenate arenes, while it should be for 0.2 equiv. of tin. This is also in agreement with the results obtained from the titration of hydrides on the surface of Ru/PVP/Sn samples, which showed a decrease with increasing tin amounts, as the result of surface coverage by tin. For the Ru/dppb/Sn, only a small amount of tin complex is required to block the faces and therefore the arene hydrogenation ability, while the olefin hydrogenation ability is preserved up to important tin loading.

Conclusions

In summary, this work shows that the surface chemistry of pre-formed Ru nanoparticles stabilized by a polymer or a diphosphine ligand can be easily modified by a simple surface organometallic reaction using a tri-n-butyltin hydride complex and leading to tin-decorated nanoparticles. In the case of Ru/PVP system it is possible to vary the amount of tin deposited on the Ru surface while in the case of dppb-stabilized RuNPs, the reaction with the tin precursor is limited by the surface coverage induced by the coordination of the bulky diphosphine ligand. The resulting modification of the ruthenium metallic surface leads to a tuning of the surface properties of the nanoparticles, as observed through the coordination of CO as well as the catalytic hydrogenation of styrene.

Experimental section

General procedures and reagents

All operations were carried out using standard Schlenk tube or Fischer-Porter bottle techniques or in a glove-box under argon atmosphere.

Solvents were purified just before use by distillation under argon atmosphere: THF and pentane (SDS) through filtration on a column in a purification apparatus (Braun). Bis(diphenylphosphino)butane (dppb), polyvinylpyrrolidone (PVP), tri-n-butyltin hydride, were purchased from Aldrich, tri-n-octyltin hydride from TCI, [Ru(COD)(COT)] from Nanomeps in Toulouse, CO and H_2 from Air Liquid, ^{13}CO (^{13}C, 99.14%) from Eurisotop. All chemicals were used without further purification.

Specimen for TEM analysis were prepared in a glove-box, by slow evaporation of a drop of each crude colloidal solution deposited onto a holey carbon covered copper grid. The TEM experiments were performed at the "Service Commun de Microscopie Electronique de l'Université Paul Sabatier" (UPS-TEMSCAN) on a JEOL JEM 1011 CX-T electron microscope operating at 100 kV with a point resolution of 4.5Å. The approximation of the particles mean size was made through a manual analysis of enlarged micrographs by measuring a number of particles on a given grid.

Wide-angle X-ray scattering (WAXS) was performed at the CEMES-CNRS. All samples were sealed in 1mm diameter Lindemann glass capillaries. The measurements of the X-ray intensity scattered by the samples irradiated with graphite-monochromatized molybdenum K_α (0.071069 nm) radiation were performed using a dedicated two-axis diffractometer. Radial distribution functions (RDF) were obtained after Fourier Transformation of the reduced intensity functions.

All solid-state NMR measurements were performed at room temperature using a Bruker Avance 400 spectrometer equipped with a 4 mm triple resonance probe CPMAS H-F/X/Y with insert for ^{31}P. The corresponding resonance frequencies are 100.49 MHz for ^{13}C, 161.75 MHz for ^{31}P and 149.03 MHz for ^{119}Sn at 9.4 Tesla. ^{13}C NMR experiments were carried out

employing MAS and CP MAS techniques at spinning rates of 10 and 12 kHz. The CP MAS spectra were recorded utilizing ramped CP-MAS sequences. Contact times were set to 3 ms and spinal 64 [15] decoupling was applied during data acquisition. Spectra were referenced to TMS. ^{1}H-^{13}C CP-MAS NMR experiments are based on the transfer of polarization from ^{1}H to ^{13}C nuclei, thus leading to an increase of the carbon signals if hydrogen atoms are in close proximity. Such experiments can be applied to determine the presence of hydrogen atoms from ligands nearby a molecule such as CO which does not contain protons. ^{31}P NMR experiments were arranged employing MAS and CP MAS techniques at spinning rates of 8 kHz, 10 kHz and 12 kHz respectively, using a recycle delay of 10 s. The recorded spectra were referenced to H_3PO_4. ^{119}Sn NMR experiments were performed under CP MAS conditions at 10 kHz. Contact times were set to 6 ms and a recycle delay of 5 s was utilized. For referencing, the external standard $Sn(chex)_4$ was set to δ=97 ppm with respect to $SnMe_4$. Measurements were carried out in a 4 mm ZrO_2 rotor.
Gas chromatograms were obtained on a HP5890 Series II Gas Chromatograph with a SGE BP1 non polar 100% dimethylpolysiloxane capillary column of (50 m x 0.32 mm x 0.25µm). The method used for 2-norbornene/norbornane experiments and styrene hydrogenation consists in 3 minutes at 80°C and a ramp of 10°C/min until 250°C.
IRFT Spectra were recorded on a Bruker Alpha-T spectrometer in the range 4000-400 cm^{-1}. All the samples were prepared as KBr pellets.
^{119}Sn Mössbauer spectra were recorded at room temperature in the transmission mode on a standard EG&G spectrometer in the constant acceleration mode by using a $Ca^{119\,m}SnO_3$ source of 10 mCi nominal activity. The velocity scale was calibrated by means of a room temperature spectrum of α-Fe recorded with a ^{57}Co-(Rh) source. The δ (isomer shift) and Δ (quadrupole splitting) hyperfine parameters were determined by fitting the Lorentzian lines to the experimental data using the ISO program.[16] All isomer shifts are given with respect to the room temperature $BaSnO_3$ spectrum. The effective thickness of all absorbers was in the 0.5−1.0 mg ^{119}Sn cm^{-2} range. The cell was then neutralized and sealed under primary vacuum. Further technical details are provided in the Supporting Information.

Computational details

All computations were performed within the framework of the spin-polarized density functional theory (DFT). The exchange-correlation potential was approximated by the generalized gradient approach proposed by Perdew, Burke, and Ernzerhof (PBE) [17]. Calculation of the energetic parameters, as well as the geometry optimizations were carried out using the projector augmented waves (PAW) full-potential reconstruction [18] implemented in the Vienna *ab initio* simulation package VASP [19]. After careful analysis of the *k*-points sampling, we found that a kinetic energy cutoff of 500 eV was necessary to achieve a total energy convergence within several millielectronvolts. For the geometry optimizations, a (5×5×1) Γ-centered [20] *k*-points grid was used to sample the reciprocal space combined with a Gaussian smearing of 0.2 eV width for the partial occupancies. Atoms were free to move until the residual forces on any direction were less than 0.05 eV/Å. The geometry was then refined with a smearing of 0.02 eV and a geometry optimization threshold of 0.02 eV/ Å. To yield accurate energy differences, we used a (9×9×1) k-points grid and the tetrahedron method proposed by Blöchl [21] for the *k*-space integration. A (4×4) cell of the Ru(0001) surface was modeled by a slab of 6 layers separated to its periodic images in the *z* direction by a vacuum of 19.2 Å for a total cell height of 30 Å. It is slightly higher than the (2×2) cell previously defined for the study of hydrides adsorption on the same surface [22]. The number of layers and the vacuum height were tested and proven to be sufficient to model accurately the surface for a reasonable computational cost.
The theoretical titration of tin ligands on the surface was done using a home-made program, dressNPs, which is a part of a multiscale strategy aiming at decorating the surface of metal NPs with ligands. The algorithm implemented in dressNPs is related to a coarse-grained method, the metal core and the ligands being kept frozen during this process. Within this virtual CPK model, a steric hindrance index is minimized in order to find the optimal number of ligands that could be grafted on the surface without being sterically discomforted. The relative orientations and positions of the ligands are adjusted at every step by a Monte-Carlo process. A small set of different ligands can eventually be simultaneously introduced on the surface. The geometry of each type of ligand was separately optimized at the DFT-B3PW91 functional implemented in Gaussian03,[i] using a 6-31G(*d,p*) basis set. [23] Regarding the metal core, we considered a 1.9 nm hcp RuNP (262 Ru atoms: 167 on the surface and 95 inner atoms). Among the $HSnBu_3$ isomers differing by the relative orientations of butyl arms, we found two structures separated by less than 2 kcal/mol at the DFT-B3PW91 level of calculation. The three -Bu groups in the lowest one are horizontally stretched out. They lie vertically in the higher one, slightly reducing their steric range with respect to the lowest one. Owing to the possible fluxionality of the -Bu arms, the two conformations for $-SnBu_3$ were considered in our process. The Ru-Sn bond length was set up to the one optimized in $SnMe_3$*, 3H* (compounds **1** and **1'**, see text). A similar strategy was applied for -SnBu, which was grafted on μ_3 sites.

Synthesis of Ru/PVP or dppb/Sn Nanoparticles

Ru/PVP and Ru/dppb nanoparticles were synthesized following methods previously described. [6a,7b] Details are given hereafter:
Ru/PVP/Sn: Ru(COD)(COT) (157 mg, 0.50 mmol) was introduced in a Fischer-Porter bottle and left under vacuum for 30 min. A solution of PVP (1g) in THF (60 mL), degassed by freeze-pump cycles, was then added using a transfer tubing. The resulting yellow solution was stirred for 30 min at room temperature, after which the bottle was pressurized under 3 bar dihydrogen and the solution allowed reacting for 68 h. During this time a black precipitate of Ru/PVP was formed. After

elimination of excess dihydrogen a solution of tri-n-butyltin hydride (13.5µL, 0.05 mmol, 0.1 equiv.) in THF (10 mL) was added to the colloidal solution of Ru/PVP under magnetic stirring. After 18 h, the solution was concentrated to 20 mL and filtrated by cannula. The precipitate was washed with pentane (3 x 30 mL) and dried overnight. Elemental analysis (Fluorescence X) Sn/Ru = 0.2.

Ru/dppb/Sn: Ru(COD)(COT) (154 mg, 0.49 mmol) was introduced in a Fischer-Porter bottle and left in vacuum for 30 min. THF (100 mL) degassed, by three freeze-pump cycles, were then added. The resulting yellow solution was cooled to 193K and a solution of dppb (20.8 mg, 0.049 mmol, 0.1 equiv.) in THF (60 mL) was introduced into the bottle. The Fischer-Porter bottle was pressurized under 3 bar dihydrogen and the solution was left to warm slowly to room temperature under vigorous stirring. After 24 h a homogenous black solution (colloidal Ru/dppb) was obtained, and the excess dihydrogen was eliminated. A solution of tri-n-butyltin hydride (13 µL, 0.049 mmol, 0.1 equiv.) in THF (10 mL) was added to the colloidal solution of Ru/dppb under stirring. After 18 h, the solution was concentrated to 20 mL and filtrated by cannula. The precipitate was washed with pentane (3 x 30 mL) and dried overnight. Elemental analysis (Fluorescence X) Sn/Ru = 0.1.

Quantification of hydrides at the surface of nanoparticles

The general procedure for the preparation of reaction mixtures for the quantification of hydrogen atoms adsorbed onto the surface of Ruthenium nanoparticles by GC analyses was carried out following a previously described procedure [24]. Each colloidal solution has been prepared in THF. On each fresh colloidal solution, five cycles of 1 min vacuum/ 1 min bubbling of argon were performed to eliminate dissolved dihydrogen from solution. Then, 1.0 equiv. of olefin (2-norbornene) was added. Samples were regularly taken from the solutions (after 18 h) for GC analyses and estimation of the olefins conversion into alkanes. To get nanoparticles-free solutions, filtration of the samples was realized through an Al_2O_3 pad.

We considered nanoparticles mean sizes and surface ruthenium atom contents as following: Ru/PVP/Sn NPs (mean size: 1.5 nm / 75% surface atoms) and for Ru/dppb/Sn NPs (mean size: 1.7 nm/ 50% surface atoms).

Reaction with CO

Solid samples of Ru/PVP/Sn or Ru/dppb/Sn nanoparticles were introduced in a Fischer-Porter bottle. The reactor was pressurized with 3 bar of H_2 for 6h to remove traces of oxygen from the surface. The Fischer-Porter bottle was then evacuated for 15 min after which it was pressurized with 1 bar of ^{13}CO. The nanoparticles were left during 18h time at room temperature under an atmosphere of ^{13}CO. Then, the gas was evacuated for 20 min and the sample was transferred in a rotor for ^{13}C NMR experiments in the solid state.

Surface reactivity with styrene

In a typical experiment, 0.03 mmol of total metal Ru nanoparticles were introduced into a Fisher-Porter reactor under an argon atmosphere. Then, 5 ml of THF and 1 ml of styrene, which were degassed before use, were added and there action mixture was pressurized to 3 bar H_2. Aliquots were taken from the reaction medium at different reaction times and analyzed by GC to evaluate the reactivity of the nanoparticles.

Acknowledgements

The authors thank V. Collière and L. Datas at UPS-TEMSCAN for electron microscopy facilities. We also acknowledge financial support from CNRS, ANR (SIDERUS BLAN-08-0010-03) and ANR-DFG (MOCANANO 2011-INTB-1011-1) projects, Interreg Sudoe (TRAIN2 project) and the European Union for ERC Advanced Grant (NANOSONWINGS 2009-246763). TG thanks the CNRS-MPG cooperation for financial support for a postdoctoral stay in France. RP thanks the HPCs CALcul en MIdi-Pyrénées (CALMIP-Hyperion, grant P0611) and the Grand Equipement National de Calcul Intensif (GENCI-TGCC-Curie, grant 6211) for generous allocations of computer time.

Notes and references

[a] Laboratoire de Chimie de Coordination; CNRS; LCC; 205 Route de Narbonne, F-31077 Toulouse, France ; karine.philippot@lcc-toulouse.fr

[b] Université de Toulouse; UPS, INPT; LCC; F-31077 Toulouse, France.

[c] LPCNO; Laboratoire de Physique et Chimie des Nano-Objets, UMR5215 INSA-CNRS-UPS, Institut des Sciences appliquées, 135, Avenue de Rangueil, F-31077 Toulouse, France ; chaudret@insa-toulouse.fr

[d] CNRS ; Centre d´Elaboration de Matériaux et d´Etudes Structurales (CEMES) ; 29, rue Jeanne Marvig, BP 4347, 31055 Toulouse Cedex, France.

[e] Institut Charles Gerhardt, ICG/AIME (UMR 5253 CNRS), Université Montpellier II CC 15-02, Place E. Bataillon, 34095 Montpellier Cedex 5, France.

1. a) *Clusters and Colloids. From Theory to Applications*, (Ed: G. Schmid), WILEY-VCH, Weinheim, 1994; b) B. Zhou, S. Han, R. Raja, G. Somorjai in *Nanotechnology in Catalysis*, ed. Kluwer Academic/Plenum Publisher, New York, 2003; c) H. Ulrich, L. Uzi (Eds), *Nanocatalysis*, Springer, Series Nanoscience and Technology, 2007; d) *Nanoparticles and Catalysis*, (Ed: D. Astruc), WILEY-INTERSCIENCE, New York, 2008; e) Concepts in Nanocatalysis, K. Philippot and P. Serp, in *Nanomaterials in Catalysis* P. Serp and K. Philippot (Eds.), WILEY-VCH, Weinheim, 2013, **1**, 1-54.
2. a) Organometallic Derived–I: Metals,Colloids and Nanoparticles, K. Philippot and B. Chaudret, in *Comprehensive Organometallic Chemistry III*, R.H. Crabtree & M.P. Mingos (Eds-in-Chief), Elsevier, Volume 12 – Applications III: Functional Materials, Environmental and Biological Applications, Dermot O'Hare (Volume Ed.), 2007, **12**, 71-99 ; b) C. Amiens, B. Chaudret, D. Ciuculescu-Pradines, V. Collière, K. Fajerwerg, P. Fau, M. Kahn, A. Maisonnat, K.Philippot, *New J. Chem.*, *2013*, **37** (11), 3374 – 3401.
3. P. Lara, K. Philippot, B. Chaudret, *Chem.Cat.Chem*, 2013, **5**, 28-45 and references therein.

4. G. Beamson, A. J. Papworth, C. Philipps, A. M. Smith, R. Whyman, *J. Catal*., 2010, **269**, 93–102
5. a) J. P. Candy, A. El Mansour, O. A. Ferretti, G. Mabilon, J. P. Bournonville, J. M. Basset, G. Martino, *J. Catal.*, 1988, **112**, 201-209; b) J. P. Candy, O. A. Ferretti, G. Mabilon, J. P. Bournonville, A. El Mansour, J. M. Basset, G. Martino, *J. Catal*., 1988, **112**, 210-220; c) M. Agnelli, P. Louessard, A. El Mansour, J. P. Candy, J. P. Bournonville, J. M. Basset, *Catalysis Today*, 1989, **6**, 63-72; d) P. Louessard, J. P. Candy, J. P. Bournonville, J. M. Basset, *Stud. Surf. Sci. Catal*., 1989, **48**, 591-600; e) F. Humblot, D. Didillon, F. Lepeltier, J. P. Candy, J. Corker, O. Clause, F. Bayard, J. M. Basset, *J. Am. Chem. Soc.*, 1998, **120**, 137-146.
6. a) F. Novio, K. Philippot, B. Chaudret, *Catal. Lett.* 2010, **140**, 1-7 ; b) F. Novio, D. Monahan, Y. Coppel, G. Antorrena, P. Lecante, K. Philippot, B. Chaudret, *Chemistry A. Eur. J.*, 2014, **20**, 1287-1297.
7. a) C. Pan, K. Pelzer , K. Philippot, B. Chaudret, F. Dassenoy, P. Lecante, M. J. Casanove, *J. Am. Chem. Soc*., 2001, **123**, 7584-7593; b) J. Garcia-Anton, M. R. Axet, S. Jansat, K. Philippot, B. Chaudret, T. Pery, G. Buntkowsky, H. H. Limbach, *Angew. Chem. Int. Ed*. 2008, **47**, 2074-2078.
8. L. Eriksson, J. Lanner, *Acta Crist*., 2001, **E57**, 85-86.
9. J. Stievano, *Phys. Chem. B*,1999**, 103**, 9545-9556.
10. a) T.M. Duncan, K.W. Zilm, D.M. Hamilton, T.W. Root, *J.Phys.Chem*., 1989, **93**, 2583-2590 ; b) J.S. Bradley,J.M. Millar, E.W. Hill, S. Behal, B. Chaudret, A. Duteil, *Faraday Discuss*, 1991, **92**, 255-268; c) A. Duteil, R. Quéau, B. Chaudret, R. Mazel, C. Roucau, Chem. Mater., 1993, **5**, 341-347; d) S. E. Shore, J. P. Ansermet, C. P. Slichter, J. H. Sinfelt, *Phys. Rev. Lett.*,1987, **58**, 953–956; e) J. P. Ansermet, C. P. Slichter, J. H. Sinfelt, *J. Chem. Phys*., 1988, **88**, 5963-5971; f) L. R. Becerra, C. A. Klug, C. P. Slichter, J. H. Sinfelt, *J. Chem. Phys.*, 1993, **97**, 12014-12019.
11. a) T. Pery, K. Pelzer, G. Buntkowski, K. Philippot, H. H. Limbach, B. Chaudret, *Chem.Phys.Chem.*, 2005, **6**, 605–607; b) F. Schröder, D. Esken, M. Cokoja, M. W. E. Van den Berg, O. Lebedev, G. Van Tendeloo, B. Walaszek, G. Buntkowsky, H. H. Limbach, B. Chaudret, R. A. Fischer, *J. Am. Chem. Soc.*,2008, **130**, 6119–6130; c) A. Adamczyk, Y. Xu, B. Walaszek, F. Roelofs, T. Pery, K. Pelzer, K. Philippot, B. Chaudret, H. H. Limbach, H. Breitzke, G. Buntkowsky, *Top.Catal.*,2008, **48**, 75–83; d) T. Gutmann, E. Bonnefille, H. Breitzke, P.-J. Debouttière, P.-J., K. Philippot, R. Poteau, G. Buntkowsky, B. Chaudret, *Phys. Chem. Chem. Phys.*, 2013, **15**, 17383-17394; e) T. Gutmann, I. del Rosal, B. Chaudret, R. Poteau, H.-H. Limbach, G. Buntkowsky, *Chem. Phys. Chem.*, 2013, **14**, 3026-3033.
12. L. A. Truflandier, I. del Rosal, B. Chaudret, R. Poteau, I. C. Gerber, *Chem.Phys.Chem.*, 2009, **10**, 2939-2942.
13. a) P. Lara, O. Rivada-Wheelaghan, S. Conejero, R. Poteau, K. Philippot, B. Chaudret, *Angew. Chem. Int. Ed.*2011, **123**, 12286-12290; b) P. Lara, M. J. Casanove, P. Lecante, P-F. Fazzini, K. Philippot, B. Chaudret, *J. Mater. Chem.*,2012, **22**, 3578-3584; c) P. Lara, T. Ayvali, M. J. Casanove, P. Lecante, A. Mayoral, P-F. Fazzini, K. Philippot, B. Chaudret, *Dalton Trans.*,2013, **42**, 372-382.
14. *Nanoparticles*, G. Schmid (Ed.) Wiley-VCH, Weinheim, 2004.
15. B. M. Fung, A. K. Khitrin, K. Ermolaev, *J. Magn. Reson.*, 2000, **142**, 97-101.
16. W. Kundig, *Nucl. Instrum. Methods*,2012, **75**, 336-340.
17. a) J. P. Perdew, K. Burke, M. Ernzerhof, *Phys. Rev. Lett.*,1996, **77**, 3865-3868; b) J. P. Perdew, K. Burke, M. Ernzerhof, *Phys. Rev. Lett.*,1997, **78**, 1396.
18. P. Blöchl, *Phys. Rev. B*, 1994, **50**,17953-17979; b) G. Kresse, D. Joubert, *Phys. Rev. B*, 1999, **59**,1758-1775.
19. G. Kresse, J. Fürthmuller, *Phys. Rev. B*, 1996, **54**,11169-11186; b) G. Kresse, J. Fürthmuller, *Comput. Mater. Sci*.,1996, **6**, 15-50.
20. H. J. Monkhorst, J. D. Pack, *Phys. Rev. B*, 1976, **13**, 5188-5192.
21. P. E. Blöchl, O. Jepsen, O. K. Andersen, *Phys. Rev. B*, 1994, **49**, 16223-16233.
22. I. del Rosal, L. A. Truflandier, R. Poteau, I. C. Gerber, *J. Phys. Chem. C*, 2011, **115**, 2169-2178.
23. Frisch, M. J. et al. (**2003**). *Gaussian 03 (Revision B.05)*.
24. F. Humblot, D. Didillon, F. Lepeltier, J.P. Candy, J. Corker, O. Clause, F. Bayard, J.M. Basset, *J. Am. Chem. Soc*.,1998, **120**, 137-146.

Table of Content entry (1 sentence of maximum 20 words)

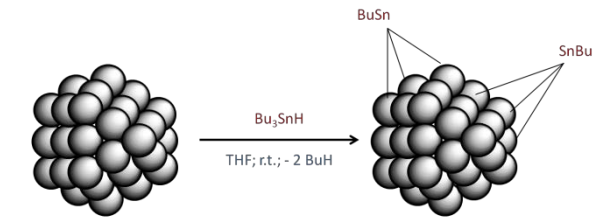

PVP- or dppb-stabilized RuNPs
PVP= polyvinylpyrrolidone; dppb=diphenylphosphinobutane

Spectroscopic techniques and theoretical calculations allowed to characterize μ^3-bridging "SnR" groups on ruthenium nanoparticle surface after reaction with Bu_3SnH.